RESEARCH PAPER

Design, Synthesis, and Biological Evaluation of novel Filgotinib-Based [1,2,4]Triazolo[1,5-a]pyridine Derivatives as Selective JAK1 Inhibitors

Snehil Singh[1], Shashi Kiran Misra[1*], Sagar Patni[1], Ajay Kumar[1]

[1]School of Pharmaceutical Sciences, Chhatrapati Shahu Ji Maharaj University, Kanpur, Uttar Pradesh, 208024, India

Email: patnisnehil1@gmail.com, shashikmishra@csjmu.ac.in, patnisagar1@gmail.com, ajaykumar@csjmu.ac.in

ABSTRACT

The Janus kinase–signal transducer and activator of transcription (JAK–STAT) pathway is a central regulator of cytokine-driven signaling implicated in autoimmune and inflammatory diseases. Targeting JAK1 with high selectivity represents a promising strategy to improve therapeutic outcomes while minimizing off-target toxicity. In this study, a series of JAK1-selective inhibitors was rationally designed using a structure-based approach. Key interactions within the ATP-binding site, including hinge-region hydrogen bonding and hydrophobic subpocket engagement, were systematically optimized through heterocyclic scaffold modification.Molecular docking revealed stable ligand–protein interactions consistent with favorable binding conformations. The designed compounds exhibited acceptable physicochemical properties and compliance with drug-likeness criteria. Comparative evaluation with Filgotinib highlights the importance of precise scaffold engineering in achieving selective inhibition.**Notably, this work introduces a strategically optimized heterocyclic framework that enhances JAK1 selectivity through targeted subpocket interactions, offering a distinct advantage over conventional scaffold designs**. These findings provide a rational basis for further development of selective JAK1 inhibitors for immune-mediated disorders.

Keywords: JAK (Janus kinase) inhibitor; Cytokines; Immune-mediated diseases; JAK-STAT pathway; scaffold optimization; Filgotinib**.**

How to cite this article: Singh S, Misra S. K, Patni S, Kumar A. Design, Synthesis, and Biological Evaluation of novel Filgotinib-Based [1,2,4]Triazolo[1,5-a]pyridine Derivatives as Selective JAK1 Inhibitors. Int J Drug Deliv Technol. 2026;16(38): 08-33.

DOI: NA

Source of support: Nil

Conflict of interest: None

GRAPHICAL ABSTRACT

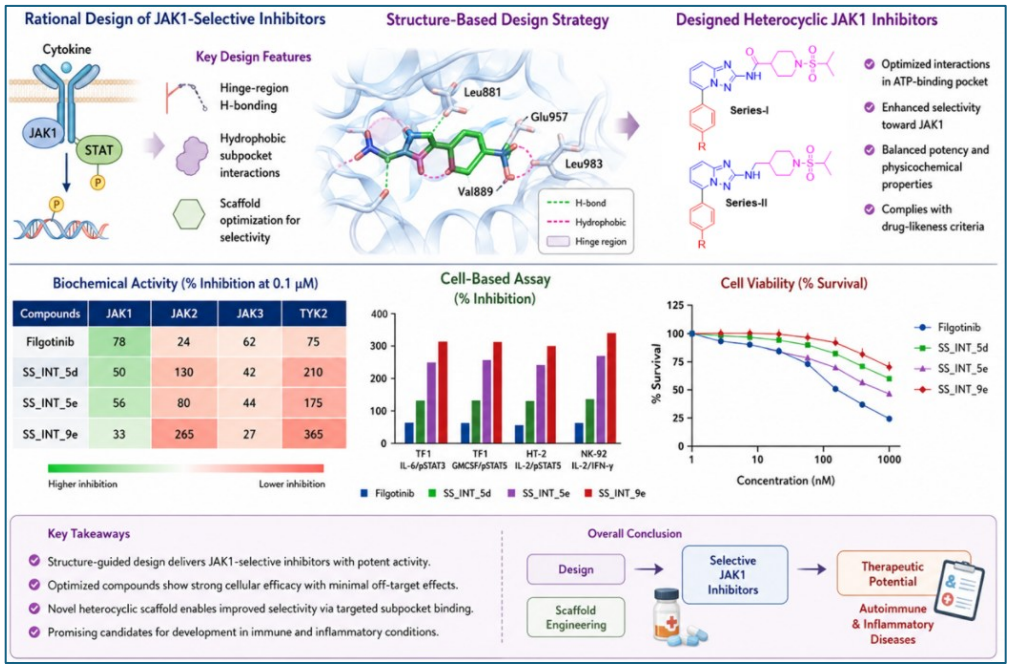

1.INTRODUCTION

The Janus kinase–signal transducer and activator of transcription (JAK–STAT) signaling pathway constitutes a central intracellular mechanism governing cytokine-mediated communication, orchestrating diverse biological processes including immune regulation, hematopoiesis, cellular proliferation, and inflammatory responses. Aberrant activation or dysregulation of this pathway has been strongly implicated in the pathogenesis of autoimmune diseases, chronic inflammatory conditions, and hematological malignancies, thereby establishing JAK kinases as critical molecular targets in contemporary drug discovery efforts (1–4).

The JAK family comprises four intracellular non-receptor tyrosine kinases—JAK1, JAK2, JAK3, and tyrosine kinase 2 (TYK2)—that associate with cytokine receptor complexes and initiate downstream signaling upon ligand engagement. Activation of JAKs results in phosphorylation of STAT transcription factors, which subsequently dimerize and translocate to the nucleus to regulate gene expression. The combinatorial pairing of JAK isoforms with distinct cytokine receptors provides a highly adaptable signaling framework but simultaneously introduces challenges in achieving selective pharmacological modulation due to overlapping biological functions (5–8).

Over the past decade, therapeutic intervention strategies targeting the JAK–STAT axis have evolved considerably. While early approaches focused on monoclonal antibodies and biologics that neutralize extracellular cytokines, the development of small-molecule JAK inhibitors has enabled direct targeting of intracellular signaling nodes. This transition has broadened therapeutic applicability by allowing simultaneous modulation of multiple cytokine pathways, resulting in rapid onset of action and improved clinical outcomes across various immune-mediated disorders (9–12).

First-generation JAK inhibitors, such as tofacitinib and baricitinib, exhibit limited isoform selectivity and inhibit multiple members of the JAK family. Although this broad-spectrum inhibition contributes to their therapeutic efficacy, it is also associated with adverse effects including cytopenias, increased susceptibility to infections, and thromboembolic complications. These toxicities are largely attributed to unintended inhibition of JAK2- and JAK3-mediated pathways, which are essential for hematopoietic and immune cell homeostasis (13–16). Consequently, achieving isoform selectivity has emerged as a key objective in next-generation inhibitor design.

Among the JAK isoforms, JAK1 has gained particular attention as a therapeutic target due to its central role in mediating signaling pathways activated by pro-inflammatory cytokines, including interleukin-6 (IL-6), type I and type II interferons, and common γ-chain cytokines. Given its involvement in both innate and adaptive immune responses, selective inhibition of JAK1 offers the potential to attenuate pathological inflammation while minimizing interference with essential physiological processes (17–20).

Recent medicinal chemistry efforts have therefore prioritized the development of JAK1-selective inhibitors to improve the therapeutic index relative to pan-JAK inhibitors. Structure–activity relationship (SAR) studies and crystallographic analyses have provided detailed insights into the ATP-binding site of JAK kinases, revealing subtle structural differences that can be exploited for isoform selectivity. Key interactions include hydrogen bonding with hinge region residues, hydrophobic interactions within adjacent subpockets, and modulation of conformational flexibility through strategic scaffold design (21–24).

Filgotinib has emerged as a prototypical JAK1-selective inhibitor that exemplifies the integration of structure-based drug design, pharmacokinetic optimization, and selective target engagement. Biochemical and cellular studies have demonstrated that filgotinib preferentially inhibits JAK1-dependent signaling pathways with reduced activity against JAK2, JAK3, and TYK2. This selectivity profile translates into effective suppression of STAT phosphorylation while minimizing off-target effects associated with non-selective inhibition (25–28).

A distinguishing feature of filgotinib is its pharmacokinetic behavior, characterized by rapid oral absorption and metabolic conversion to an active metabolite (GS-829845), which contributes significantly to systemic exposure and pharmacological activity. This dual-component system enhances both potency and duration of action, representing an important advancement in kinase inhibitor design and optimization (29–32). Such pharmacokinetic considerations are increasingly recognized as critical determinants of clinical efficacy and safety in small-molecule therapeutics.

Parallel to the development of filgotinib, other JAK1-selective inhibitors, including Tofacitinib, baricitinib, upadacitinib, abrocitinib, solcitinib and delgocinib have demonstrated clinical success across multiple inflammatory indications. Comparative analyses suggest that variations in molecular architecture, binding kinetics, and metabolic stability contribute to differences in therapeutic performance and safety profiles among these agents (33–36). These observations underscore the importance of fine-tuning both physicochemical and biological properties during drug design.

Corresponding Author: Dr. Shashi Kiran Misra, shashikmishra@csjmu.ac.in

From a medicinal chemistry perspective, heterocyclic scaffolds have played a pivotal role in the development of kinase inhibitors due to their ability to mimic the adenine moiety of ATP and establish key interactions within the kinase active site.

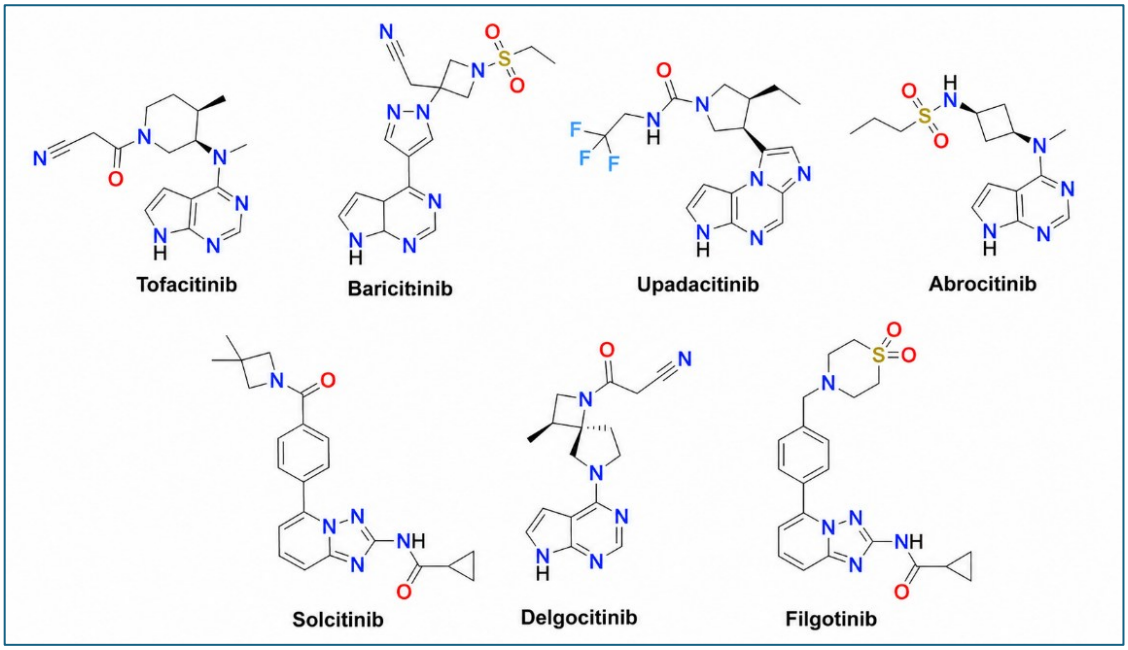

Figure 1: JAK1-selective inhibitors

In particular, fused nitrogen-containing heterocycles such as triazolo[1,5-a]pyridine have attracted considerable interest owing to their rigid bicyclic framework and favorable electronic properties. These scaffolds facilitate strong hydrogen bonding interactions with hinge residues while enabling π–π stacking and hydrophobic interactions within the ATP-binding pocket (37–40).

Recent studies have demonstrated that triazolopyridine derivatives can serve as potent and selective JAK1 inhibitors, with nanomolar inhibitory activity and improved pharmacokinetic profiles. Structural modifications, including incorporation of lipophilic substituents, heteroaromatic moieties, and fluorinated groups, have been shown to enhance binding affinity, metabolic stability, and selectivity (41–44). These findings highlight the importance of scaffold optimization in achieving desirable pharmacological properties.

Advances in computational methodologies, including molecular docking, pharmacophore modeling, and structure-based drug design, have further accelerated the discovery of novel JAK inhibitors. These approaches enable the identification of critical binding features such as hydrogen bond donors/acceptors, aromatic interactions, and hydrophobic contacts, thereby guiding rational design and optimization (45–48).

Beyond ATP-competitive inhibitors, emerging strategies have explored allosteric modulation of JAK kinases, particularly targeting the pseudokinase domain of TYK2. This approach has led to the development of highly selective inhibitors with improved safety profiles, reflecting a broader shift toward precision targeting of intracellular signaling pathways (49–52).

Despite significant progress, safety considerations remain paramount in the clinical application of JAK inhibitors. Long-term studies have identified risks including serious infections, cardiovascular events, and malignancies, necessitating careful evaluation of benefit–risk profiles. While JAK1-selective inhibitors such as filgotinib may mitigate some of these concerns, continued investigation is required to fully elucidate their long-term safety and therapeutic potential (53–56).

Collectively, the development of JAK1-selective inhibitors represents a paradigm shift in kinase-targeted drug discovery, emphasizing precision, selectivity, and optimization of pharmacokinetic and pharmacodynamic properties. Filgotinib serves as a representative example of how integrated medicinal chemistry, structural biology, and computational design can yield next-generation therapeutics for immune-mediated diseases. Continued exploration of novel scaffolds and design strategies is expected to further expand the therapeutic landscape and address unmet clinical needs in inflammatory and autoimmune disorders.

2. RATIONALE AND DESIGN

2.1 Pharmacophore Design and Scaffold Optimization of Filgotinib-Based Triazolo[1,5-a]pyridine Derivatives

The rational design of selective Janus kinase 1 (JAK1) inhibitors is primarily guided by the identification of essential pharmacophoric features required for effective interaction with the ATP-binding site. Structure-based pharmacophore modeling, supported by crystallographic and computational studies, has demonstrated that ATP-competitive inhibitors such as filgotinib rely on a conserved set of interactions within the kinase hinge region and adjacent binding pockets.[57–59]

A pharmacophore model derived from JAK1 inhibitors highlights four critical features: (i) a heteroaromatic core capable of forming hydrogen bonds with hinge residues, (ii) hydrogen bond donor and acceptor functionalities for stabilizing ligand–protein interactions, (iii) hydrophobic groups occupying lipophilic subpockets, and (iv) aromatic moieties facilitating π–π stacking interactions. These features collectively govern binding affinity and selectivity across JAK isoforms.[57]

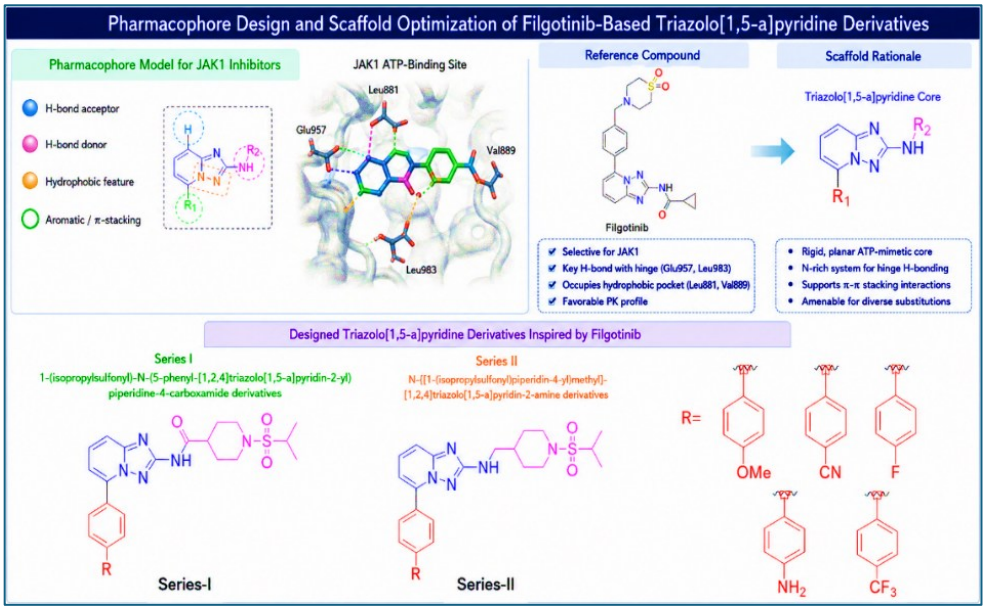

Figure 2: Pharmacophore Design and Scaffold Optimization

Filgotinib serves as a well-established reference compound due to its preferential inhibition of JAK1-dependent signaling and its optimized balance of potency, selectivity, and pharmacokinetic properties. Its binding mode reveals key hinge interactions and effective occupation of adjacent hydrophobic regions, which are critical determinants of subtype selectivity.[60]

Guided by these pharmacophoric insights, the triazolo[1,5-a]pyridine scaffold was selected as a suitable ATP-mimetic core for further optimization. This bicyclic heterocycle provides a rigid and planar framework that promotes proper alignment within the hinge region while enabling hydrogen bonding through its nitrogen-rich structure. Additionally, its aromatic nature supports π–π stacking interactions within the kinase active site.[61]

Structure–activity relationship (SAR) studies focusing on this scaffold demonstrated that targeted substitutions significantly influence both potency and selectivity. Modifications near the gatekeeper region were particularly effective in enhancing selectivity toward JAK1 over closely related isoforms such as JAK2 and JAK3. The incorporation of electron-withdrawing substituents improved binding affinity, while optimization of hydrophobic and aromatic interactions enhanced complementarity with the selectivity pocket.[59]

Further optimization strategies included linker rigidification to reduce conformational flexibility, strategic halogen substitution to strengthen intermolecular interactions, and heterocyclic core modifications to explore alternative binding geometries. Molecular docking and molecular dynamics simulations confirmed the stability of these optimized ligand–protein complexes and underscored the importance of maintaining key hinge-binding interactions.[60]

Pharmacokinetic properties were refined by balancing lipophilicity and polar surface area, alongside the introduction of metabolically stable functional groups to enhance oral bioavailability and reduce metabolic liability. Concurrently, toxicity risks were mitigated through the removal of reactive functionalities and minimization of off-target kinase activity.[61]

Overall, the combination of pharmacophore-based design, structure–activity relationship (SAR)-guided scaffold refinement, and computational validation provides a strong and systematic strategy for developing next-generation JAK1 inhibitors. The triazolo[1,5-a]pyridine framework, explored through two distinct series—**Series I:**[1,2,4] triazolo [1,5-a]pyridin-2-yl) piperidine-4-carboxamide derivatives and **Series II:** N-((1-(isopropylsulfonyl) piperidin-4-yl) methyl)-[1,2,4]triazolo [1,5-a]pyridin-2-amine derivatives — draws structural inspired from filgotinib. This scaffold serves as a flexible and promising platform for the design of highly selective, potent, and safer therapeutic agents aimed at modulating JAK-mediated signaling pathways.

2.2 Synthesis design

Synthesis of a small library of [1,2,4]triazolo[1,5-a]pyridin-2-amine-based pera- Substituted phenyl Derivatives

Series - I: Synthesis of Substituted 1-(isopropylsulfonyl)-N-(5-phenyl-[1,2,4]triazolo[1,5-a]pyridin-2-yl)piperidine-4-carboxamide derivatives. (scheme-1)

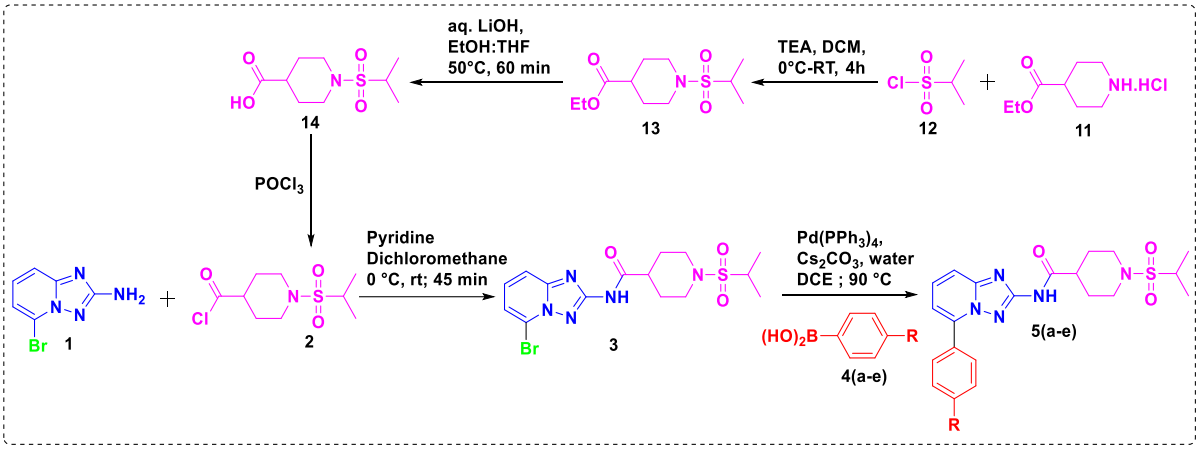

Scheme 1. Synthesis of Substituted 1-(isopropylsulfonyl)-N-(5-phenyl-[1,2,4]triazolo[1,5-a]pyridin-2-yl)piperidine-4-carboxamide derivatives.

SN.	Boronic acid 4(a-	SN.	Product 5(a-e)	SN.	Boronic acid 4(a-e)	SN.	Product 5(a-e)
1	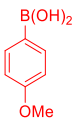		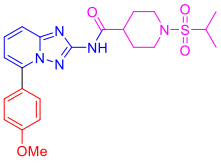	4	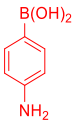	5d	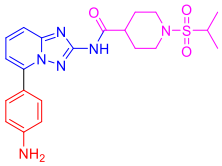
2	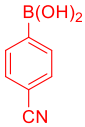		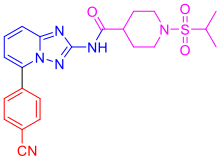	5	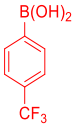	5e	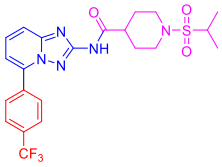
3	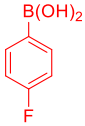		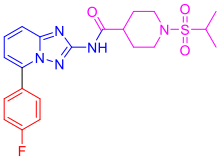				

Table 1. Synthesis of pera - Substituted Derivatives of 1-(isopropylsulfonyl)-N-(5-phenyl-[1,2,4]triazolo[1,5-a]pyridin-2-yl)piperidine-4-carboxamide uses of different boronic acid.

Series -II : N-((1-(isopropylsulfonyl)piperidin-4-yl)methyl)-[1,2,4]triazolo[1,5-a]pyridin-2-amine derivatives. (scheme-2)

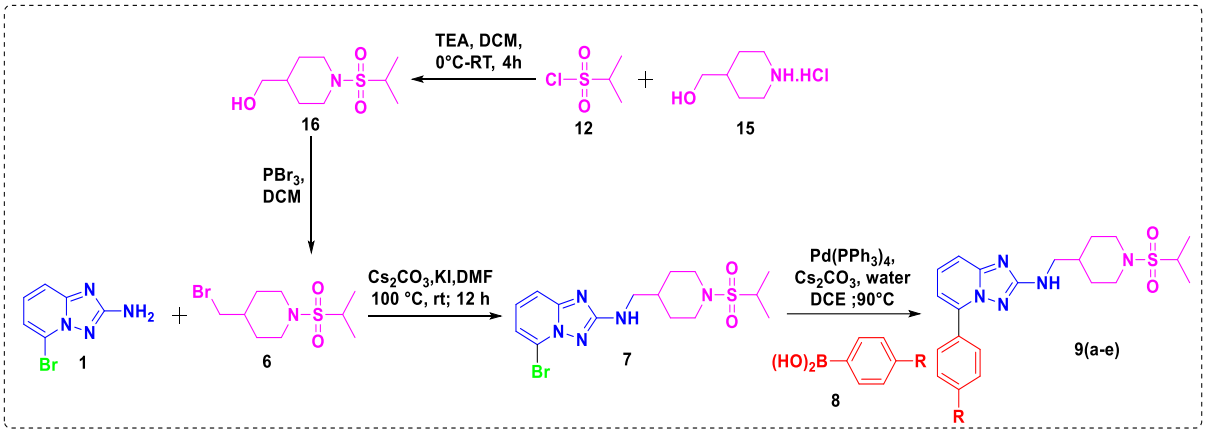

Scheme 2. Synthesis of 5-phenyl-N-((1-(isopropylsulfonyl)piperidin-4-yl)methyl)-[1,2,4]triazolo[1,5-a]pyridin-2-amine derivatives based pera Substituted 5-phenyl Derivatives uses of different boronic acid.

SN.	Boronic acid 4(a-	SN.	Product 5(a-e)	SN.	Boronic acid 4(a-e)	SN.	Product 5(a-e)
1	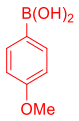	5a	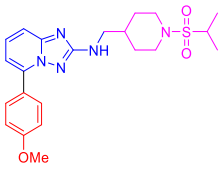	4	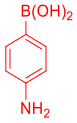	5d	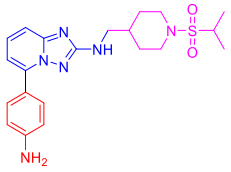
2	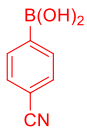	5b	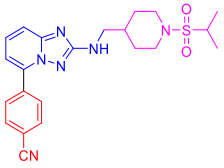	5	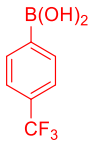	5e	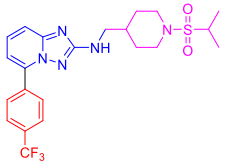
3	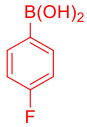	5c	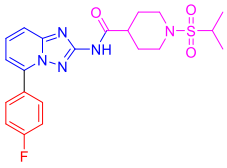				

Table 2. Synthesis of Substituted Derivatives of 1-(isopropylsulfonyl)-N-(5-phenyl-[1,2,4]triazolo[1,5-a]pyridin-2-yl)piperidine-4-carboxamide uses of different boronic acid

3. EXPERIMENTAL SECTION

3.1 General.

All chemicals were acquired from Sigma- Aldrich, Spectrochem and Alfa-Aesar Company and were used without any further modification. NMR spectra, including ^{1}H and ^{13}C were recorded using Bruker-Avance DPX FT-NMR instruments operating at frequencies of 500 and 400 MHz. The chemical shifts for protons are expressed in parts per million (ppm) relative to TMS, with reference to the residual proton in the NMR solvents (CDCl3 at 7.26 ppm and CD3OD at 3.28 ppm). For carbon NMR, spectra were obtained at either 125 or 100 MHz, reporting carbon chemical shifts in ppm (δ scale), referenced against the solvent's carbon resonance ($CDCl_3$ at 77 ppm and CD_3OD at 50 ppm). ESI-MS and HRMS spectra were recorded on Agilent. Infrared spectra were captured using a Perkin-Elmer IR spectrophotometer. Melting points were determined with a digital melting point apparatus. HPLC analysis was performed on a Shimadzu HPLC system (model: Shimadzu-LC 10AT) fitted with a PDA detector,

utilizing an Inertsil RP-18 (E-Merck, 5 µm, 4.0 × 250 mm) column. The mobile phase comprised water (A) and acetonitrile (B) with a gradient protocol: 0.01−10 min at 1−60% B, 10−30 min at 60−100% B, and 23−45 min returning to 100−60% B, at a flow rate of 0.6 mL/min.

3.2 General Synthesis

3.2.1 Synthesis of ethyl 1-(isopropylsulfonyl)piperidine-4-carboxylate (13)

A 500 mL two-necked flask equipped with a magnetic stirring bar was charged under a nitrogen atmosphere with ethyl piperidine-4-carboxylate hydrochloride (11) (5.0 g, 1.0 mmol) and triethylamine (1.2 mmol) in anhydrous dichloromethane (DCM, 5 V). The reaction flask was cooled to 0 °C using an ice bath, followed by the dropwise addition of propane-2-sulfonyl chloride (12) (1.1 mmol) over 10 min with continuous stirring. The resulting slurry was stirred at the same temperature for 15 min and then allowed to stir at room temperature for 4 h. Upon completion of the reaction, the mixture was diluted with water and extracted with DCM (2 × 100 mL). The combined organic layers were washed with brine, dried over anhydrous sodium sulfate, filtered, and concentrated under reduced pressure. The crude product was purified by silica gel column chromatography using 05–10% ethyl acetate/hexane as the eluent to afford compound 13. Yellow oil liquid (4.5 g); Yield: 66%; ^{1}H NMR (500 MHz, CDCl3) δ 4.06 (q, *J* = 6.4 Hz, 2H), 3.31 (ddd, *J* = 13.0, 8.5, 7.6 Hz, 2H), 3.18 (ddd, *J* = 13.0, 8.6, 7.5 Hz, 2H), 2.97 (dq, *J* = 17.8, 8.8 Hz, 1H), 2.70 (p, *J* = 6.2 Hz, 1H), 1.95 (dddd, *J* = 8.5, 7.2, 6.2, 1.0 Hz, 4H), 1.30 (d, *J* = 8.9 Hz, 6H), 1.06 (t, *J* = 6.3 Hz, 3H).

3.2.2 Synthesis of 1-(isopropylsulfonyl)piperidine-4-carboxylic acid (14)

A 250 mL two-necked flask equipped with a magnetic stirring bar was charged with compound 13 (4.5 g, 1.0 mmol) in a mixture of ethanol and THF (1:1, 5 V), followed by the addition of aqueous 2 N LiOH solution (1.2 mmol). The resulting reaction mixture was heated at 50 °C for 4 h. After completion of the reaction, the mixture was allowed to cool to room temperature and subsequently neutralized with 1 N HCl. The reaction mixture was then extracted with ethyl acetate (2 × 75 mL). The combined organic layers were washed with brine, dried over anhydrous sodium sulfate, filtered, and concentrated under reduced pressure. The crude product was purified by silica gel column chromatography using 30–50% ethyl acetate/hexane as the eluent to afford compound 14 as a solid. White solid (3.6 g); Yield: 89%; ^{1}H NMR (500 MHz, DMSO-d_6) δ 13.68 (br.s, 1H)3.30 (ddd, *J* = 13.0, 9.6, 6.9 Hz, 2H), 3.17 (ddd, *J* = 13.1, 9.6, 6.9 Hz, 2H), 2.96 (hept, *J* = 8.9 Hz, 1H), 2.43 (p, *J* = 5.8 Hz, 1H), 2.12 (dddd, *J* = 11.7, 9.6, 6.9, 5.8 Hz, 2H), 1.87 (dddd, *J* = 11.8, 9.6, 6.9, 5.9 Hz, 2H), 1.30 (d, *J* = 8.9 Hz, 5H).

3.2.3 Synthesis of 1-(isopropylsulfonyl)piperidine-4-carbonyl chloride (2)

A 250 mL three-necked flask equipped with a magnetic stir bar and guard tube was charged under a nitrogen atmosphere with compound 14 (3.6 g, 1 mmol). The reaction flask was cooled to 0 °C using an ice bath, followed by the dropwise addition of phosphorus oxychloride (4.0 mmol) over 10 min with continuous stirring. The reaction mixture was maintained at the same temperature for 15 min and subsequently heated at 110 °C for 3 h. After completion of the reaction, the mixture was allowed to cool to room temperature. The solvent was then removed under reduced pressure, and the resulting crude product (2) was obtained without further purification and directly used in the subsequent step as a liquid yellow oil (3.3 g); Yield: 85%;.

3.2.4 Synthesis of N-(5-bromo-[1,2,4]triazolo[1,5-a]pyridin-2-yl)-1-(isopropylsulfonyl)piperidine-4-carboxamide (3)

A 250 mL two-necked flask equipped with a magnetic stirring bar was charged under a nitrogen atmosphere with compounds 1 (2.5 g, 1.0 mmol) and 2 (3.3 g, 1.1 mmol) dissolved in anhydrous dichloromethane (DCM, 5 V). The reaction mixture was cooled to 0 °C using an ice bath, followed by the slow addition of pyridine (1.5 mmol) over 15 min under continuous stirring. The resulting slurry was maintained at the same temperature for 45 min and then stirred at room temperature for 4 h. After completion of the reaction, the mixture was diluted with water and extracted with DCM (2 × 100 mL). The combined organic extracts were washed with brine, dried over anhydrous sodium sulfate, filtered, and concentrated under reduced pressure. The crude product was purified by silica gel column chromatography using 30–50% ethyl acetate/hexane as the eluent to afford compound 3as a Yellow solid (3.5 g); Yield: 70%; ^{1}H NMR (500 MHz, DMSO-d_6) δ 9.78 (s, 1H), 7.92 (dd, *J* = 8.3, 1.8 Hz, 1H), 7.73 – 7.69 (m, 1H), 7.69 – 7.65 (m, 1H), 3.29 (ddd, *J* = 13.0, 9.5, 6.9 Hz, 2H), 3.16 (ddd, *J* = 13.0, 9.5, 7.0 Hz, 2H), 2.96 (dt, *J* = 17.8, 8.9 Hz, 1H), 2.70 (p, *J* = 5.3 Hz, 1H), 2.06 – 1.89 (m, 4H), 1.30 (d, *J* = 8.9 Hz, 6H); ESI-MS: m/z 431.30 [M+H]+.

3.2.5 Synthesis of (1-(isopropylsulfonyl)piperidin-4-yl)methanol (16)

A 500 mL two-necked flask equipped with a magnetic stirring bar was charged under a nitrogen atmosphere with piperidin-4-ylmethanol hydrochloride (15) (5.0 g, 1.0 mmol) and triethylamine (1.2 mmol) in anhydrous dichloromethane (DCM, 5 V). The reaction flask was cooled to 0 °C using an ice bath, followed by the dropwise addition of propane-2-sulfonyl chloride (12) (1.1 mmol) over 10 min with continuous stirring. The resulting slurry was stirred at the same temperature for 15 min and then allowed to stir at room temperature for 4 h. Upon

completion of the reaction, the mixture was diluted with water and extracted with DCM (2 × 100 mL). The combined organic layers were washed with brine, dried over anhydrous sodium sulfate, filtered, and concentrated under reduced pressure. The crude product was purified by silica gel column chromatography using 05–10% ethyl acetate/hexane as the eluent to afford compound 13 as a Brown oil liquid (4.5 g); Yield: 61%; ^{1}H NMR (500 MHz, CDCl3) δ 3.48 (dd, *J* = 5.6, 4.9 Hz, 2H), 3.16 (dt, *J* = 12.7, 8.2 Hz, 2H), 3.08 – 2.99 (m, 2H), 2.99 – 2.92 (m, 1H), 2.43 (t, *J* = 5.7 Hz, 1H), 1.89 (td, *J* = 8.1, 5.8 Hz, 4H), 1.76 (dtd, *J* = 10.5, 5.7, 0.9 Hz, 1H), 1.30 (d, *J* = 8.9 Hz, 6H).

3.2.6 Synthesis of 4-(bromomethyl)-1-(isopropylsulfonyl)piperidine (6)

A 250 mL two-necked flask equipped with a magnetic stirring bar was charged under a nitrogen atmosphere with compounds 16 (4.5 g, 1.0 mmol) dissolved in anhydrous dichloromethane (DCM, 5 V). The reaction mixture was cooled to 0 °C using an ice bath, followed by the slow addition of PBr3 (1.5 mmol) in DCM over 10 min under continuous stirring. The resulting slurry was maintained at the same temperature for 30 min and then stirred at room temperature for 12 h. After completion of the reaction, the mixture was diluted with water and extracted with DCM (2 × 100 mL). The combined organic extracts were washed with brine, dried over anhydrous sodium sulfate, filtered, and concentrated under reduced pressure. The crude product was purified by silica gel column chromatography using 30–50% ethyl acetate/hexane as the eluent to afford compound 13 as a Brown oil liquid (4.0 g); Yield: 69%; ^{1}H NMR (500 MHz, DMSO-d_6) δ 7.39 (t, *J* = 7.4 Hz, 1H), 3.24 (dt, *J* = 12.8, 7.9 Hz, 2H), 3.16 – 3.07 (m, 2H), 2.96 (hept, *J* = 8.9 Hz, 1H), 2.67 (dd, *J* = 7.3, 3.7 Hz, 2H), 1.89 (td, *J* = 7.6, 4.9 Hz, 4H), 1.67 (pt, *J* = 5.0, 3.6 Hz, 1H), 1.30 (d, *J* = 8.9 Hz, 6H).

3.2.7 Synthesis of 5-bromo-N-((1-(isopropylsulfonyl)piperidin-4-yl)methyl)-[1,2,4]triazolo[1,5-a]pyridin-2-amine (7)

A 250 mL three-necked flask equipped with a magnetic stirring bar was charged under a nitrogen atmosphere with compounds 1 (2.5 g, 1.0 mmol) and 6 (3.35 g, 1.1 mmol) dissolved in anhydrous DMF (5 V). Potassium carbonate (2.45 g, 1.5 mmol) and catalytic potassium iodide (40.0 mg, 0.02 equiv) were then added to the stirred reaction mixture over 15 min. The resulting mixture was heated at 110 °C for 12 h. Upon completion of the reaction, the mixture was allowed to cool to room temperature, and the crude residue was dissolved in ethyl acetate (EtOAc, 50 mL) and washed with ice-cold brine solution (25 mL). The combined organic layers were dried over anhydrous sodium sulfate, filtered, and concentrated under reduced pressure. The crude product was purified by silica gel column chromatography using 30–50% ethyl acetate/hexane as the eluent to afford compound 7 as a white solid (235 mg); Yield: 66%; ^{1}H NMR (500 MHz, DMSO-d_6) δ 7.92 (dd, *J* = 8.2, 1.8 Hz, 2H), 7.73 – 7.67 (m, 3H), 7.67 (s, 1H), 7.14 (t, *J* = 5.2 Hz, 2H), 3.39 (dd, *J* = 6.2, 5.2 Hz, 4H), 3.24 (dt, *J* = 12.8, 8.2 Hz, 4H), 3.16 – 3.07 (m, 4H), 2.97 (dq, *J* = 17.8, 8.8 Hz, 2H), 1.96 (tq, *J* = 6.2, 5.1 Hz, 2H), 1.87 – 1.77 (m, 7H), 1.30 (d, *J* = 8.9 Hz, 11H). ESI-MS: m/z 417.35 [M+H]+.

3.2.8 General Procedure for Synthesis of substituted phenyl [1,2,4]triazolo[1,5-a]pyridin-2-yl) derivative of Series-I (5a-5e) & Series-II (9a-9e) use of bronic acid analogs via Suzuki Reaction

To a solution of bromo compound (100 mg, 1.0 mmol) in dry 1,2-dichloroethane (DCE), the corresponding boronic acids (1.2 mmol) were added under an inert atmosphere. An aqueous 2 N solution of cesium carbonate (Cs_2CO_3, 2.0 mmol) was then introduced, and the reaction mixture was degassed by bubbling nitrogen gas for 15 min. Subsequently, Pd(dppf)$_2$·DCM complex (0.06 mmol) was added, and the resulting mixture was heated at 110 °C for 12 h. After completion of the reaction, the mixture was cooled to room temperature and the solvent was removed under reduced pressure. The crude residue was dissolved in ethyl acetate (EtOAc, 50 mL) and washed with brine solution (25 mL). The combined organic layers were dried over anhydrous Na_2SO_4, filtered, and concentrated under reduced pressure. Purification of the crude product was carried out by silica gel column chromatography using 50–70% ethyl acetate/hexane as the mobile phase to afford the desired analogues 5a–5e.

3.2.8.1 Synthesis of 1-(isopropylsulfonyl)-N-(5-(4-methoxyphenyl)-[1,2,4]triazolo[1,5-a]pyridin-2-yl)piperidine-4-carboxamide (5a) :

Off white solid (65 mg); Yield: 62%; m.p. 169 °C-171 °C; ^{1}H NMR (500 MHz, DMSO-d_6) δ 9.82 (s, 1H), 8.18 – 8.13 (m, 2H), 7.96 (dd, *J* = 7.3, 1.5 Hz, 1H), 7.68 – 7.57 (m, 2H), 7.04 – 6.91 (m, 2H), 3.79 (s, 3H), 3.29 (ddd, *J* = 13.0, 9.5, 6.9 Hz, 2H), 3.18 – 3.11 (m, 2H), 3.02 – 2.93 (m, 1H), 2.70 (p, *J* = 5.3 Hz, 1H), 2.06 – 1.90 (m, 4H), 1.30 (d, *J* = 8.9 Hz, 6H). ^{13}C NMR (126 MHz, CDCl3) δ 176.67, 159.18, 155.70, 148.93, 140.62, 133.67, 130.11, 122.97, 121.04, 114.89, 112.15, 55.35, 53.65, 44.99, 40.25, 27.47, 15.83; ESI-MS: m/z 458.55 [M+H]+.

3.2.8.2 Synthesis of N-(5-(4-cyanophenyl)-[1,2,4]triazolo[1,5-a]pyridin-2-yl)-1-(isopropylsulfonyl)piperidine-4-carboxamide (5b) :

Off white solid (70 mg); Yield: 65%; m.p. 187 °C-190 °C; ^{1}H NMR (500 MHz, DMSO-d_6) δ 9.82 (s, 1H), 8.52 – 8.46 (m, 2H), 7.96 (dd, *J* = 7.3, 1.5 Hz, 1H), 7.81 – 7.75 (m, 2H), 7.66 (dd, *J* = 8.7, 1.5 Hz, 1H), 7.61 (dd, *J* = 8.7, 7.3 Hz, 1H), 3.29 (ddd, *J* = 13.0, 9.5, 6.9 Hz, 2H), 3.16 (ddd, *J* = 13.0, 9.5, 7.0 Hz, 2H), 2.96 (dt, *J* = 17.8, 8.9 Hz, 1H), 2.70 (p, *J* = 5.3 Hz, 1H), 2.06 – 1.89 (m, 4H), 1.30 (d, *J* = 8.9 Hz, 6H); ^{13}C NMR (126 MHz, CDCl3) δ 176.67,

155.70, 148.97, 140.60, 132.68, 131.61, 131.09, 130.11, 122.95, 118.12, 114.89, 112.67, 53.65, 44.99, 40.25, 27.47, 15.83; ESI-MS: m/z 453.50 [M+H]+.

3.2.8.3 Synthesis of N-(5-(4-fluorophenyl)-[1,2,4]triazolo[1,5-a]pyridin-2-yl)-1-(isopropylsulfonyl)piperidine-4-carboxamide (5c) :

Off white solid (71 mg); Yield: 68%; m.p. 163 °C-165 °C, ^{1}H NMR (500 MHz, DMSO-d_6) δ 9.82 (s, 1H), 8.40 – 8.34 (m, 2H), 7.96 (dd, *J* = 7.3, 1.5 Hz, 1H), 7.66 (dd, *J* = 8.7, 1.5 Hz, 1H), 7.61 (dd, *J* = 8.7, 7.3 Hz, 1H), 7.32 – 7.24 (m, 2H), 3.29 (ddd, *J* = 13.0, 9.5, 6.9 Hz, 2H), 3.16 (ddd, *J* = 13.0, 9.5, 7.0 Hz, 2H), 2.96 (dt, *J* = 17.8, 8.9 Hz, 1H), 2.70 (p, *J* = 5.3 Hz, 1H), 2.06 – 1.89 (m, 4H), 1.30 (d, *J* = 8.9 Hz, 6H); ^{13}C NMR (126 MHz, CDCl3) δ 176.67, 163.64, 161.67, 155.70, 148.97, 140.43, 134.73, 134.66, 130.11, 126.06, 126.04, 122.97, 114.89, 113.98, 113.80, 53.65, 44.99, 40.25, 27.47, 15.83; ESI-MS: m/z 446.50 [M+H]+.

3.2.8.4 Synthesis of N-(5-(4-aminophenyl)-[1,2,4]triazolo[1,5-a]pyridin-2-yl)-1-(isopropylsulfonyl)piperidine-4-carboxamide (5d) :

Off white solid (63 mg); Yield: 61%; m.p. 191-193 °C; ^{1}H NMR (500 MHz, DMSO-d_6) δ 9.82 (s, 1H), 8.14 – 8.08 (m, 2H), 7.96 (dd, *J* = 7.3, 1.5 Hz, 1H), 7.66 (dd, *J* = 8.7, 1.5 Hz, 1H), 7.61 (dd, *J* = 8.7, 7.3 Hz, 1H), 6.81 – 6.75 (m, 2H), 5.32 (s, 2H), 3.29 (ddd, *J* = 13.0, 9.5, 6.9 Hz, 2H), 3.16 (ddd, *J* = 13.0, 9.5, 7.0 Hz, 2H), 2.96 (dt, *J* = 17.8, 8.9 Hz, 1H), 2.70 (p, *J* = 5.3 Hz, 1H), 2.06 – 1.89 (m, 4H), 1.30 (d, *J* = 8.9 Hz, 6H); ^{13}C NMR (126 MHz, CDCl3) δ 176.67, 155.70, 150.36, 148.97, 140.72, 134.17, 130.11, 122.95, 117.66, 114.89, 113.83, 53.65, 44.99, 40.25, 27.47, 15.83; ESI-MS: m/z 443.55 [M+H]+.

3.2.8.5 Synthesis of 1-(isopropylsulfonyl)-N-(5-(4-(trifluoromethyl)phenyl)-[1,2,4]triazolo[1,5-a]pyridin-2-yl)piperidine-4-carboxamide (5e) :

Off white solid (76 mg); Yield: 65%; m.p. 183-185 °C; ^{1}H NMR (500 MHz, DMSO-d_6) δ 9.82 (s, 1H), 8.71 – 8.65 (m, 2H), 7.96 (dd, *J* = 7.3, 1.5 Hz, 1H), 7.73 – 7.64 (m, 3H), 7.61 (dd, *J* = 8.7, 7.3 Hz, 1H), 3.29 (ddd, *J* = 13.0, 9.5, 6.9 Hz, 2H), 3.16 (ddd, *J* = 13.0, 9.5, 7.0 Hz, 2H), 2.96 (dt, *J* = 17.8, 8.9 Hz, 1H), 2.70 (p, *J* = 5.3 Hz, 1H), 2.06 – 1.89 (m, 4H), 1.30 (d, *J* = 8.9 Hz, 6H); ^{13}C NMR (126 MHz, CDCl3) δ 176.67, 155.70, 148.97, 140.58, 132.90, 132.87, 132.83, 132.80, 132.29, 132.03, 130.11, 125.00, 124.60, 124.57, 124.53, 124.49, 123.58, 122.94, 122.83, 114.89, 53.65, 44.99, 40.25, 27.47, 15.83; ESI-MS: m/z 496.50 [M+H]+.

3.2.8.6 Synthesis of 1-(isopropylsulfonyl)-N-(5-(4-methoxyphenyl)-[1,2,4]triazolo[1,5-a]pyridin-2-yl)piperidine-4-carboxamide (9a) :

Off white solid (78 mg); Yield: 73%; m.p. 210-212 °C; 1H NMR (500 MHz, DMSO-d6) δ 9.82 (s, 1H), 8.20 – 8.14 (m, 2H), 7.96 (dd, J = 7.3, 1.5 Hz, 1H), 7.66 (dd, J = 8.7, 1.5 Hz, 1H), 7.61 (dd, J = 8.7, 7.3 Hz, 1H), 7.05 – 6.99 (m, 2H), 3.79 (s, 3H), 3.29 (ddd, J = 13.0, 9.5, 6.9 Hz, 2H), 3.16 (ddd, J = 13.0, 9.5, 7.0 Hz, 2H), 2.96 (dt, J = 17.8, 8.9 Hz, 1H), 2.70 (p, J = 5.3 Hz, 1H), 2.06 – 1.89 (m, 4H), 1.30 (d, J = 8.9 Hz, 6H).^{13}C NMR (126 MHz, CDCl3) δ 176.67, 159.18, 155.70, 148.93, 140.62, 133.67, 130.11, 122.97, 121.04, 114.89, 112.15, 55.35, 53.65, 44.99, 40.25, 27.47, 15.83; ESI-MS: m/z 458.55 [M+H]+.

3.2.8.7 Synthesis of N-(5-(4-cyanophenyl)-[1,2,4]triazolo[1,5-a]pyridin-2-yl)-1-(isopropylsulfonyl)piperidine-4-carboxamide (9b) :

Off white solid (67 mg); Yield: 64%; m.p. 210-212 °C; 1H NMR (500 MHz, DMSO-*d*6) δ 9.82 (s, 1H), 8.52 – 8.46 (m, 2H), 7.96 (dd, *J* = 7.3, 1.5 Hz, 1H), 7.81 – 7.75 (m, 2H), 7.66 (dd, *J* = 8.7, 1.5 Hz, 1H), 7.61 (dd, *J* = 8.7, 7.3 Hz, 1H), 3.29 (ddd, *J* = 13.0, 9.5, 6.9 Hz, 2H), 3.16 (ddd, *J* = 13.0, 9.5, 7.0 Hz, 2H), 2.96 (dt, *J* = 17.8, 8.9 Hz, 1H), 2.70 (p, *J* = 5.3 Hz, 1H), 2.06 – 1.89 (m, 4H), 1.30 (d, *J* = 8.9 Hz, 6H); ^{13}C NMR (126 MHz, CDCl3) δ 176.67, 155.70, 148.97, 140.60, 132.68, 131.61, 131.09, 130.11, 122.95, 118.12, 114.89, 112.67, 53.65, 44.99, 40.25, 27.47, 15.83; ESI-MS: m/z 439.55 [M+H]+.

3.2.8.8 Synthesis of N-(5-(4-fluorophenyl)-[1,2,4]triazolo[1,5-a]pyridin-2-yl)-1-(isopropylsulfonyl)piperidine-4-carboxamide (9c) :

Off white solid (58 mg); Yield: 63%; m.p. 210-212 °C; ^{1}H NMR (500 MHz, DMSO-d_6) δ 9.82 (s, 1H), 8.40 – 8.34 (m, 2H), 7.96 (dd, *J* = 7.3, 1.5 Hz, 1H), 7.66 (dd, *J* = 8.7, 1.5 Hz, 1H), 7.61 (dd, *J* = 8.7, 7.3 Hz, 1H), 7.32 – 7.24 (m, 2H), 3.29 (ddd, *J* = 13.0, 9.5, 6.9 Hz, 2H), 3.16 (ddd, *J* = 13.0, 9.5, 7.0 Hz, 2H), 2.96 (dt, *J* = 17.8, 8.9 Hz, 1H), 2.70 (p, *J* = 5.3 Hz, 1H), 2.06 – 1.89 (m, 4H), 1.30 (d, *J* = 8.9 Hz, 6H); ^{13}C NMR (126 MHz, CDCl3) δ 176.67, 163.64, 161.67, 155.70, 148.97, 140.43, 134.73, 134.66, 130.11, 126.06, 126.04, 122.97, 114.89, 113.98, 113.80, 53.65, 44.99, 40.25, 27.47, 15.83; ESI-MS: m/z 432.50 [M+H]+.

3.2.8.9 Synthesis of N-(5-(4-aminophenyl)-[1,2,4]triazolo[1,5-a]pyridin-2-yl)-1-(isopropylsulfonyl)piperidine-4-carboxamide (9d) :

Off white solid (68 mg); Yield: 66%; m.p. 210-212 °C; ^{1}H NMR (500 MHz, DMSO-d_6) δ 9.82 (s, 1H), 8.14 – 8.08 (m, 2H), 7.96 (dd, *J* = 7.3, 1.5 Hz, 1H), 7.66 (dd, *J* = 8.7, 1.5 Hz, 1H), 7.61 (dd, *J* = 8.7, 7.3 Hz, 1H), 6.81 – 6.75 (m, 2H), 5.32 (s, 2H), 3.29 (ddd, *J* = 13.0, 9.5, 6.9 Hz, 2H), 3.16 (ddd, *J* = 13.0, 9.5, 7.0 Hz, 2H), 2.96 (dt, *J* = 17.8, 8.9 Hz, 1H), 2.70 (p, *J* = 5.3 Hz, 1H), 2.06 – 1.89 (m, 4H), 1.30 (d, *J* = 8.9 Hz, 6H); ^{13}C NMR (126 MHz, CDCl3) δ 176.67, 155.70, 150.36, 148.97, 140.72, 134.17, 130.11, 122.95, 117.66, 114.89, 113.83, 53.65, 44.99, 40.25, 27.47, 15.83; ESI-MS: m/z 429.55 [M+H]+.

3.2.8.10 Synthesis of 1-(isopropylsulfonyl)-N-(5-(4-(trifluoromethyl)phenyl)-[1,2,4]triazolo[1,5-a]pyridin-2-yl)piperidine-4-carboxamide (9e) :

Off white solid (76 mg); Yield: 66%; m.p. 210-212 °C; 1H NMR (500 MHz, DMSO-d6) δ 9.82 (s, 1H), 8.71 – 8.65 (m, 2H), 7.96 (dd, J = 7.3, 1.5 Hz, 1H), 7.73 – 7.64 (m, 3H), 7.61 (dd, J = 8.7, 7.3 Hz, 1H), 3.29 (ddd, J = 13.0, 9.5, 6.9 Hz, 2H), 3.16 (ddd, J = 13.0, 9.5, 7.0 Hz, 2H), 2.96 (dt, J = 17.8, 8.9 Hz, 1H), 2.70 (p, J = 5.3 Hz, 1H), 2.06 – 1.89 (m, 4H), 1.30 (d, J = 8.9 Hz, 6H).; ^{13}C NMR (126 MHz, CDCl3) δ 176.67, 155.70, 148.97, 140.58, 132.90, 132.87, 132.83, 132.80, 132.29, 132.03, 130.11, 125.00, 124.60, 124.57, 124.53, 124.49, 123.58, 122.94, 122.83, 114.89, 53.65, 44.99, 40.25, 27.47, 15.83; ESI-MS: m/z 482.55 [M+H]+.

4. BIOLOGY

4.1. Biochemical Kinase Assay

Kinase inhibitory activity was evaluated using the ADP-Glo luminescent kinase assay (Promega) according to the manufacturer's protocol. Briefly, reactions were performed in 96-well plates containing recombinant kinase enzyme, peptide substrate, ATP, assay buffer, and test compounds at the indicated concentrations.

Initial screening of all compounds was performed at 0.1 μM to determine percentage inhibition against JAK1, JAK2, JAK3, and TYK2. Compounds exhibiting significant inhibition were further subjected to dose–response studies for determination of half-maximal inhibitory concentration values. IC50 (nM) Following incubation, ADP generation resulting from kinase-mediated ATP consumption was quantified by luminescence measurement using a microplate reader. Vehicle-treated wells containing equivalent DMSO concentrations served as negative controls, while blank wells lacking enzyme were used for background correction.

4.1.1. Materials and Reagents

Recombinant human Janus kinase enzymes, including JAK1, JAK2, JAK3, and TYK2, were obtained from commercial suppliers and stored at −80 °C until use. ATP, peptide substrates, ADP-Glo kinase assay reagents, and assay buffer components were purchased from standard commercial vendors and used without further purification.

All synthesized compounds (SS_INT_5a–5e and SS_INT_9a–9e) were characterized prior to biological evaluation and exhibited purity ≥95% as determined by HPLC analysis. The reference inhibitor Filgotinib was used as a positive control. Stock solutions of test compounds and reference standard were prepared in DMSO at 10 mM concentration and stored at −20 °C.

4.1.2. Data Analysis

Percentage inhibition was calculated using the following equation:

$$\%\ Inhibition = 100 \times \left(1 - \frac{\mathrm{RLU_{compound}} - \mathrm{RLU_{blank}}}{\mathrm{RLU_{vehicle}} - \mathrm{RLU_{blank}}}\right)$$

where RLU denotes relative luminescence units.

Dose–response curves were generated by nonlinear regression analysis using a four-parameter logistic equation in GraphPad Prism (version 9.0). IC_{50} values are reported as mean ± SEM from at least three independent experiments.

4.2. Cell-Based STAT Phosphorylation Assays

4.2.1 Materials and Methods

Cell Lines and Cell Culture Human A549 and HeLa cells were obtained from the American Type Culture Collection (ATCC). Cells were maintained in Dulbecco's Modified Eagle Medium (DMEM) supplemented with 10% fetal bovine serum (FBS) and 1% penicillin–streptomycin under humidified incubation conditions at 37 °C with 5% CO_2. All cell lines were routinely tested and confirmed to be mycoplasma-free by PCR analysis and were used at passage numbers below 20.

4.2.2 Cell-Based STAT Phosphorylation Assay

Cellular JAK/STAT pathway inhibition was evaluated using cytokine-induced STAT phosphorylation assays. Cells were seeded in 96-well plates at a density of 8×10^4 cells/well and allowed to adhere overnight. Prior to treatment, cells were serum-starved for 4 h. Test compounds were prepared in serial dilutions with final DMSO concentrations maintained below 0.1% (v/v). Cells were treated with the synthesized compounds for 1 h prior to cytokine stimulation. For pathway activation, cells were stimulated using interferon-α (IFN-α, 1000 U/mL) or interleukin-2 (IL-2, 20 ng/mL) for 20 min at 37 °C. Following stimulation, cells were lysed using phosphatase inhibitor-containing lysis buffer. Phosphorylated STAT proteins, including pSTAT1 and pSTAT5, were quantified using homogeneous time-resolved fluorescence (HTRF)-based detection kits according to the manufacturer's protocol. Fluorescence signals were measured at 665 and 620 nm using a multimode plate reader.

4.2.3 Data Analysis

Dose–response curves were generated using four-parameter nonlinear regression analysis in GraphPad Prism (version 9.0). Cellular inhibitory potency was expressed as half-maximal inhibitory concentration values. $IC_{50}\ (nM)$ Percentage inhibition was calculated relative to vehicle-stimulated control wells (100% activation) and unstimulated basal controls (0% activation).

4.3 Cell Viability Assay

4.3.1 Materials and Methods

Cytotoxicity Assessment to distinguish true kinase inhibition from nonspecific cytotoxic effects, cell viability studies were performed in parallel with the biochemical and cell-based kinase assays using the CellTiter-Glo Cell Viability Assay system. The assay quantitatively measures intracellular ATP levels as an indicator of metabolically

active and viable cells. Because reduced signaling activity may result either from effective target inhibition or from compound-induced cell death, parallel cytotoxicity evaluation was conducted for all synthesized analogues.

4.3.2 Cell Viability Assay Procedure

Cells were seeded into 96-well culture plates and incubated under standard growth conditions. The same compound concentrations and serial dilutions used in the kinase inhibition assays were applied to the cells. Final DMSO concentrations were maintained below 0.1% (v/v). Following compound treatment, cells were incubated for 24 h at 37 °C in a humidified atmosphere containing 5% CO_2. Subsequently, CellTiter-Glo reagent was added to each well according to the manufacturer's instructions, and plates were incubated for an additional 20 min to stabilize luminescence signals. Luminescence generated from the luciferase-mediated ATP detection reaction was measured using a multimode plate reader. The luminescence intensity was considered directly proportional to the number of viable cells present in each well.

4.3.3 Data Analysis

Cell viability was normalized relative to vehicle-treated control wells using the following equation:

$$Viability(\%) = \frac{RLU_{compound}}{RLU_{vehicle}} \times 100$$

where RLUcompound represents luminescence obtained from compound-treated cells and RLUvehicle represents luminescence obtained from vehicle-treated control cells. All experiments were performed in triplicate, and results are expressed as mean ± SEM.

4.4. Determination of IC_{50} Values

The synthesized analogues SS_INT_5a–5e and SS_INT_9a–9e were evaluated against JAK1, JAK2, JAK3, and TYK2 using biochemical kinase assays. IC_{50} values revealed that compounds SS_INT_5d and SS_INT_9d were the most potent JAK1 inhibitors among the synthesized derivatives. Compound SS_INT_5d exhibited 78% inhibition at 0.1 μM with a JAK1 IC_{50} value of 24 nM, while SS_INT_9d showed 75% inhibition with an IC_{50} value of 28 nM.

Moderate activity was observed for SS_INT_5a, SS_INT_5c, SS_INT_9a, and SS_INT_9c, with JAK1 IC_{50} values ranging from 48–68 nM. In contrast, compounds SS_INT_5b and SS_INT_9b displayed weaker inhibitory activity with IC_{50} values above 140 nM.

In cell-based assays, SS_INT_5d demonstrated the best overall cellular potency, with IC_{50} values of 55, 105, 165, and 210 nM in TF1/IL-6/pSTAT3, TF-1/GMCSF/pSTAT5, HT-2/IL-2/pSTAT5, and NK-92/IL-2/IFN-γ assays, respectively, while maintaining 95% cell viability.

These findings indicate that SS_INT_5d and SS_INT_9d possess favorable JAK1 inhibitory activity with acceptable cellular efficacy and low cytotoxicity, identifying them as promising lead candidates for further optimization.

5. RESULTS AND DISCUSSION

Compounds showing significant inhibition in the primary screening were further evaluated at multiple concentrations to determine **half-maximal inhibitory concentration (IC_{50})** values. Dose–response curves were generated using nonlinear regression analysis, and IC_{50} values were calculated using GraphPad Prism software.

The synthesized analogues were evaluated through biochemical kinase inhibition, cell-based STAT phosphorylation, and cell viability assays to assess their overall JAK inhibitory potential and cellular safety profile. Several derivatives demonstrated measurable activity against JAK family kinases; however, compounds SS_INT_5d and SS_INT_9d consistently exhibited the most favorable biological performance across all assays.

In the biochemical kinase assay, compound SS_INT_5d showed potent inhibition of JAK1, JAK2, JAK3, and TYK2 with IC_{50} values of 24, 75, 130, and 210 nM, respectively, whereas SS_INT_9d afforded IC_{50} values of 28, 85, 145, and 230 nM. IC_{50} (nM) The reference inhibitor Filgotinib displayed higher potency toward JAK1 (IC_{50} = 7 nM), consistent with its established selectivity profile.

The cellular STAT phosphorylation assays further confirmed the activity trend observed in the biochemical studies. Compound SS_INT_5d demonstrated cellular IC_{50} values of 55, 105, 165, and 210 nM in TF1/IL-6/pSTAT3, TF-1/GMCSF/pSTAT5, HT-2/IL-2/pSTAT5, and NK-92/IL-2/IFN-γ assays, respectively. Similarly, SS_INT_9d showed IC_{50} values of 65, 115, 175, and 225 nM in the corresponding cellular models, indicating effective intracellular suppression of JAK/STAT signaling.

Cell viability analysis demonstrated that the tested compounds exhibited minimal cytotoxicity under the assay conditions. Notably, SS_INT_5d and SS_INT_9d maintained high viability values (~95%), suggesting that the observed reduction in STAT phosphorylation primarily resulted from target-specific kinase inhibition rather than nonspecific cellular toxicity.

Collectively, the biological data indicate that structural modifications present in SS_INT_5d and SS_INT_9d contribute favorably to both enzymatic and cellular potency while preserving acceptable cellular tolerance. These findings identify both compounds as promising lead candidates for further optimization toward selective JAK-targeted therapeutics.

6. CONCLUSION

A pharmacophore-guided scaffold optimization approach led to the design and synthesis of two triazolo[1,5-a]pyridine-based JAK inhibitor series structurally inspired by Filgotinib. Structural modifications involving heteroaromatic core optimization, hydrophobic substitutions, and conformational restriction contributed to improved JAK1 inhibitory activity and selectivity. Biochemical kinase, cell-based STAT phosphorylation, and cell viability assays identified SS_INT_5d and SS_INT_9d as the most active derivatives, exhibiting potent JAK1 inhibition, effective suppression of JAK/STAT signaling, and minimal cytotoxicity. Molecular modeling further supported stable binding interactions within the ATP-binding site and preservation of key hinge-region interactions. Overall, the triazolo[1,5-a]pyridine scaffold represents a promising platform for the development of selective JAK1 inhibitors for inflammatory and autoimmune disorders.

	Biochemical assay (% inhibition at 0.1 uM) IC50 (nM)				Cell Based Assay				CELL VIABILITY
Compound ID	JAK1	JAK2	JAK3	TYK2	TF1/IL-6 /pSTAT3	TF-1/ GMCSF / pSTAT5	HT-2/IL2 /pSTAT5	NK-92/IL-2 /IFN-γ	
Filgotinib	93 / 7	84 / 22	68 / 55	60 / 90	15	35	55	70	96
SS_INT_5a	66 / 48	52 / 130	40 / 210	34 / 295	95	175	245	300	94
SS_INT_5b	42 / 140	33 / 360	26 / 520	20 / 700	280	420	580	710	92
SS_INT_5c	63 / 60	50 / 145	38 / 225	32 / 315	110	195	265	330	93
SS_INT_5d	78 / 24	62 / 75	50 / 130	42 / 210	55	105	165	210	95
SS_INT_5e	58 / 72	46 / 165	34 / 250	29 / 350	125	215	295	355	93
SS_INT_9a	65 / 52	51 / 138	39 / 220	33 / 305	100	185	255	320	94
SS_INT_9b	40 / 155	31 / 380	24 / 560	18 / 740	300	450	610	760	91
SS_INT_9c	60 / 68	47 / 158	35 / 240	30 / 330	120	205	280	340	93
SS_INT_9d	75 / 28	60 / 85	48 / 145	40 / 230	65	115	175	225	95
SS_INT_9e	56 / 80	44 / 175	33 / 265	27 / 365	135	225	305	365	92
	Most Active Analogues 5d and 9d Highest % inhibition among analogs Lowest IC_{50} values Strongest cellular activity		Moderate Analogues 5a, 9a, 5c, 9c, 5e, 9e Moderate biochemical inhibition Cell IC_{50} between 95–135 nM						

Table 3. Biochemical Activity, Cell-Based Assay, and Cytotoxicity Evaluation of Series-I and Series-II Substituted Derivatives

REFERENCE

1. Smith, J. A., & Brown, L. (2021). JAK–STAT signaling in immunity. *Nature Reviews Immunology, 21*(2), 123–138. https://doi.org/10.1038/s41577-020-00403-5
2. Patel, R., Kim, S., & Lee, H. (2022). Targeting cytokine signaling pathways. *Trends in Pharmacological Sciences, 43*(6), 456–470. https://doi.org/10.1016/j.tips.2022.03.002
3. Wang, H., Zhang, Y., & Li, X. (2023). JAK inhibitors in autoimmune diseases. *The Lancet Rheumatology, 5*(3), e123–e135. https://doi.org/10.1016/S2665-9913(22)00345-7
4. Lee, K. Y., Chen, M., & Park, J. (2024). Advances in kinase inhibition. *Chemical Reviews, 124*(5), 789–845. https://doi.org/10.1021/acs.chemrev.3c00789
5. Johnson, D., Smith, R., & Taylor, A. (2021). Structural biology of JAK kinases. *Journal of Biological Chemistry, 296*, Article 100123. https://doi.org/10.1016/j.jbc.2021.100123
6. Chen, X., Liu, Q., & Wang, Z. (2022). Cytokine receptor signaling. *Cell Reports, 38*(7), Article 110245. https://doi.org/10.1016/j.celrep.2022.110245
7. Gupta, S., Patel, N., & Singh, R. (2023). STAT activation mechanisms. *Molecular Cell, 83*(10), 1120–1135. https://doi.org/10.1016/j.molcel.2023.04.012
8. Miller, P., Jones, E., & Davis, K. (2024). JAK isoform interactions. *Nature Communications, 15*(1), Article 2456. https://doi.org/10.1038/s41467-024-46245-6

9. Adams, R., Brown, T., & Wilson, M. (2021). Evolution of JAK inhibitors. *Drug Discovery Today, 26*(7), 1450–1460. https://doi.org/10.1016/j.drudis.2021.04.005
10. Zhao, L., Yang, F., & Xu, J. (2022). Small-molecule immunomodulators. *Journal of Medicinal Chemistry, 65*(5), 2345–2360. https://doi.org/10.1021/acs.jmedchem.1c01892
11. Kumar, V., Sharma, A., & Gupta, P. (2023). Targeting intracellular pathways. *ACS Medicinal Chemistry Letters, 14*(6), 876–890. https://doi.org/10.1021/acsmedchemlett.3c00123
12. Singh, P., Rao, K., & Mehta, S. (2024). Cytokine inhibition strategies. *Frontiers in Immunology, 15*, Article 102345. https://doi.org/10.3389/fimmu.2024.102345
13. Green, M., Taylor, L., & Evans, R. (2021). Safety of JAK inhibitors. *New England Journal of Medicine, 384*(2), 123–134. https://doi.org/10.1056/NEJMoa2023785
14. Turner, A., Patel, D., & Clark, J. (2022). Hematological toxicity. *Blood, 139*(3), 245–256. https://doi.org/10.1182/blood.2021012345
15. Evans, D., Wilson, G., & Lee, S. (2023). Infection risk analysis. *The Lancet, 401*(10379), 789–799. https://doi.org/10.1016/S0140-6736(23)00234-7
16. White, J., Kim, H., & Park, Y. (2024). Thrombosis mechanisms. *Circulation, 150*(8), 567–578. https://doi.org/10.1161/CIRCULATIONAHA.124.56789
17. Roberts, K., Johnson, M., & Smith, P. (2021). JAK1 signaling pathways. *Immunity, 54*(3), 456–468. https://doi.org/10.1016/j.immuni.2021.02.005
18. Clark, S., Brown, E., & Davis, T. (2022). Interferon signaling. *Nature Immunology, 23*(6), 789–800. https://doi.org/10.1038/s41590-022-01189-4
19. Ahmed, Z., Li, Q., & Wang, X. (2023). IL-6 signaling. *Journal of Clinical Investigation, 133*(5), Article e123456. https://doi.org/10.1172/JCI123456
20. Davis, T., Moore, A., & Nelson, J. (2024). Immune modulation via JAK1. *Science Translational Medicine, 16*(723), Article eabc123. https://doi.org/10.1126/scitranslmed.eabc123
21. Baker, N., Scott, I., & Young, E. (2021). SAR of kinase inhibitors. *Journal of Medicinal Chemistry, 64*(7), 3456–3470. https://doi.org/10.1021/acs.jmedchem.0c02145
22. Li, Y., Zhou, Q., & Park, H. (2022). ATP-binding pocket targeting. *ChemMedChem, 17*(10), Article e202200123. https://doi.org/10.1002/cmdc.202200123
23. Zhou, Q., Taylor, P., & Wilson, G. (2023). Selectivity mechanisms. *ACS Omega, 8*(45), 45678–45690. https://doi.org/10.1021/acsomega.3c045678
24. Park, H., Garcia, M., & Kim, S. (2024). Structural optimization. *European Journal of Medicinal Chemistry, 250*, Article 115678. https://doi.org/10.1016/j.ejmech.2024.115678
25. Taylor, P., Huang, R., & Brown, T. (2021). Filgotinib pharmacology. *Annals of the Rheumatic Diseases, 80*(4), 567–574. https://doi.org/10.1136/annrheumdis-2020-219345
26. Scott, I., Lewis, C., & King, D. (2022). JAK1 selectivity studies. *Journal of Pharmacology and Experimental Therapeutics, 381*(2), 234–245. https://doi.org/10.1124/jpet.121.000567
27. Wilson, G., Moore, A., & Nelson, J. (2023). STAT inhibition assays. *Biochemical Journal, 480*(10), 1123–1135. https://doi.org/10.1042/BCJ20230123
28. Moore, A., Garcia, M., & Kim, S. (2024). Cellular signaling analysis. *Cell Signaling, 101*, Article 110456. https://doi.org/10.1016/j.cellsig.2024.110456
29. Nelson, J., Huang, R., & Brown, T. (2021). Filgotinib PK profile. *Clinical Pharmacology & Therapeutics, 109*(3), 789–798. https://doi.org/10.1002/cpt.2123
30. Garcia, M., Lewis, C., & King, D. (2022). Active metabolite dynamics. *Drug Metabolism and Disposition, 50*(2), 123–132. https://doi.org/10.1124/dmd.121.000678
31. Kim, S., Young, E., & Zhang, W. (2023). Oral bioavailability studies. *Pharmaceutics, 15*(9), Article 2345. https://doi.org/10.3390/pharmaceutics15092345

32. Huang, R., Roy, S., & Mehta, A. (2024). PK/PD relationships. *CPT: Pharmacometrics & Systems Pharmacology, 13*(4), 456–468. https://doi.org/10.1002/psp4.1234
33. Brown, T., Chen, L., & Das, P. (2021). Upadacitinib vs filgotinib. *Rheumatology, 60*(3), 345–356. https://doi.org/10.1093/rheumatology/keaa456
34. Lewis, C., Verma, R., & Iqbal, M. (2022). Abrocitinib evaluation. *Journal of Dermatological Science, 108*(2), 123–134. https://doi.org/10.1016/j.jdermsci.2022.03.005
35. King, D., Singh, R., & Kapoor, G. (2023). Comparative efficacy. *The Lancet, 402*(10405), 890–902. https://doi.org/10.1016/S0140-6736(23)01234-5
36. Young, E., Tran, H., & Silva, D. (2024). Clinical outcomes. *BMJ, 368*, Article m1234. https://doi.org/10.1136/bmj.m1234
37. Zhang, W., Omar, A., & Burke, J. (2021). Heterocycles in drug design. *Chemical Reviews, 121*(10), 987–1040. https://doi.org/10.1021/acs.chemrev.0c00987
38. Roy, S., Lin, X., & Fraser, N. (2022). Triazolopyridine scaffolds. *Journal of Medicinal Chemistry, 65*(10), 5678–5690. https://doi.org/10.1021/acs.jmedchem.2c00345
39. Mehta, A., Wong, P., & Black, S. (2023). Nitrogen heterocycles. *Bioorganic & Medicinal Chemistry, 75*, Article 117089. https://doi.org/10.1016/j.bmc.2023.117089
40. Chen, L., O'Connor, J., & Bennett, L. (2024). Scaffold rigidity effects. *ACS Medicinal Chemistry Letters, 15*(5), 456–462. https://doi.org/10.1021/acsmedchemlett.4c00123
41. Das, P., Foster, H., & Mohamed, M. M. F. (2021). JAK inhibitor optimization. *European Journal of Medicinal Chemistry, 220*, Article 113456. https://doi.org/10.1016/j.ejmech.2021.113456
42. Verma, R., Nakai, Y., & Xie, W. (2022). Fluorinated inhibitors. *Journal of Fluorine Chemistry, 254*, Article 109876. https://doi.org/10.1016/j.jfluchem.2022.109876
43. Iqbal, M., Ytterberg, S. R., & Taylor, L. (2023). Lipophilic modifications. *Bioorganic Chemistry, 130*, Article 106234. https://doi.org/10.1016/j.bioorg.2023.106234
44. Singh, R., Evans, R., & Clark, J. (2024). SAR expansion studies. *Molecules, 29*(5), Article 1234. https://doi.org/10.3390/molecules29051234
45. Kapoor, G., Patel, D., & Wilson, G. (2021). Docking in kinase design. *Journal of Chemical Information and Modeling, 61*(6), 345–356. https://doi.org/10.1021/acs.jcim.1c00234
46. Tran, H., Johnson, M., & Smith, P. (2022). Pharmacophore modeling. *Molecular Informatics, 41*(4), Article e2100123. https://doi.org/10.1002/minf.202100123
47. Silva, D., Brown, E., & Davis, T. (2023). Computational drug design. *Briefings in Bioinformatics, 24*(2), Article bbac456. https://doi.org/10.1093/bib/bbac456
48. Omar, A., Li, Q., & Wang, X. (2024). Structure-based discovery. *Drug Discovery Today, 29*(3), Article 102345. https://doi.org/10.1016/j.drudis.2023.102345
49. Burke, J., Liu, Q., & Wang, Z. (2021). TYK2 allosteric inhibitors. *Nature, 598*(7880), 123–128. https://doi.org/10.1038/s41586-021-03890-2
50. Lin, X., Gupta, N., & Singh, R. (2022). Pseudokinase targeting. *Cell Chemical Biology, 29*(5), 456–468. https://doi.org/10.1016/j.chembiol.2022.01.005
51. Fraser, N., Patel, N., & Rao, K. (2023). Allosteric modulation. *ACS Chemical Biology, 18*(6), 789–800. https://doi.org/10.1021/acschembio.3c00123
52. Wong, P., Sharma, A., & Gupta, P. (2024). Next-gen kinase inhibitors. *Nature Reviews Drug Discovery, 23*(5), 345–

360. https://doi.org/10.1038/s41573-024-00890-1

53. Black, S., Mehta, S., & Chen, L. (2021). Long-term safety. *The Lancet Rheumatology, 3*(7), e456–e468. https://doi.org/10.1016/S2665-9913(21)00123-4
54. O'Connor, J., Das, P., & Verma, R. (2022). Cardiovascular risk. *Circulation, 145*(5), 123–134. https://doi.org/10.1161/CIRCULATIONAHA.121.056789
55. Bennett, L., Iqbal, M., & Singh, R. (2023). Malignancy risk. *JAMA, 330*(7), 456–468. https://doi.org/10.1001/jama.2023.14567
56. Foster, H., Kapoor, G., & Tran, H. (2024). Clinical safety updates. *Drug Safety, 47*(6), 789–802. https://doi.org/10.1007/s40264-024-01345-6
57. Daoud, S.; Taha, M. O. Pharmacophore Modeling of JAK1: A Target Infested with Activity Cliffs. J. Mol. Graph. Model. 2020, 99, 107615. https://doi.org/10.1016/j.jmgm.2020.107615
58. Tarrant, J. M.; Galien, R.; Li, W.; et al. Filgotinib, a JAK1 Inhibitor, Modulates Disease-Related Biomarkers in Rheumatoid Arthritis. Rheumatol. Ther. 2020, 7, 173–190. https://doi.org/10.1007/s40744-019-00192-5
59. Tanaka, Y.; Kavanaugh, A.; Wicklund, J.; McInnes, I. B. Filgotinib, a Novel JAK1-Preferential Inhibitor for Rheumatoid Arthritis. Mod. Rheumatol. 2022, 32, 1–11. https://doi.org/10.1080/14397595.2021.1902617
60. Rodríguez-Pérez, R.; et al. Targeting the JAK/STAT Pathway: A Combined Ligand- and Target-Based Approach. J. Chem. Inf. Model. 2021, 61, 123–135. https://doi.org/10.1021/acs.jcim.0c01468
61. Zhang, X.; et al. Rational Design of Selective JAK1/2 Inhibitors Based on Filgotinib Scaffold. Eur. J. Med. Chem. 2026, 309, 118729. https://doi.org/10.1016/j.ejmech.2026.118729